49th AIAA Aerospace Sciences Meeting including the New Horizons Forum and Aerospace Exposition
4 - 7 January 2011, Orlando, Florida

AIAA 2011-676

Numerical, Experimental and Theoretical Studies on Mechanism of K-H Instability and Ring Generation behind Supersonic MVG

Yonghua Yan[1], Qin Li[2], Chaoqun Liu[3], Frank Lu[4]

University of Texas at Arlington,P.O. Box 19408 Arlington, TX 76019, USA

This paper illustrates the dominant mechanism of the ring-like vortex formation which was found generated by micro vortex generated (MVG) for shock-boundary layer interaction control by our implicit large eddy simulation (ILES) with high order accuracy and our experiment. An averaged velocity profile after MVG is taken as the base flow. The disturbed viscous incompressible and inviscit compressible stability equations have been derived in a 3D coordinates, axially symmetric in particular. After we introduced the effect of simplified spanwise counter-rotating vortices, we theoretically conclude that the structure of vortex rings behind the MVG is a consequence of the momentum deficit according to the axisymmetic instability theorem.

I. Introduction

In the supersonic ramp jets, shock boundary layer interaction (SBLI) can significantly reduce the quality of the flow field by triggering large-scale separation, causing total pressure loss, making the flow unsteady and distorting. MICRO vortex generator (VG) is a kind of low-profile passive control devices designed for the boundary layer control. Intensive computational and experimental studies have been made on it recently.

In our study, a high order LES and a wind tunnel test have been conducted for the investigation on the flow around micro vortex generator (MVG) at Mach number 2.5 and Reθ=9218 with the boundary layer momentum thickness as the reference length. An approach named monotone integrated LES (MILES) was adopted, in which the numerical dissipation is used as the sub-grid stress model. The well-known 5th order WENO[1] is applied as the basic numerical scheme in the MILES approach.

The flow field around the MVG and surrounding area has been studied in details. Further more, 3-D structure of the shocks is also obtained by our numerical simulation[2]. The ring-like vortices have been found formed and travel downstream. According to the analyses, a dynamic vortex model was developed and can be sketched in Fig.1 in the half domain. The new model can be described as follows. The dominant vortex near the MVG is the primary vortex; underneath there are first two secondary counter-rotating vortices, which will left the body surface later to become fully 3D separations by the way of spiral points in body surface, and these vortices seem to be wrapped by the primary vortex when propagating downstream; after that, a new secondary vortex will be generated under the primary vortex.

---

[1] Ph. D Candidate, Math Department, University of Texas at Arlington, Arlington, TX 76019

[2] Visiting Post Doc., Math Department, University of Texas at Arlington, Arlington, TX 76019

[3] Professor, Math Department, University of Texas at Arlington, Arlington, TX 76019, AIAA associate fellow.

[4] Professor, ME/AE Department, University of Texas at Arlington, Arlington, TX 76019,, AIAA associate fellow.
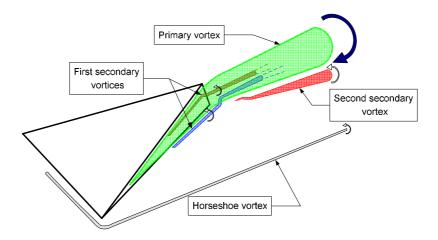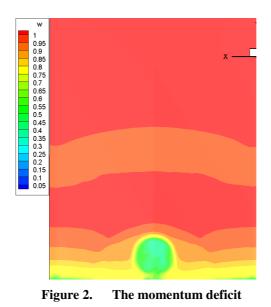
Figure 1. The dynamic vortex model

A strong momentum deficit has been found behind MVG which causes a strong circular shear layer, as shown in Fig. 2. The result is in consistency with the referenced computations and experiments[3,4,5].

Figure 2.   The momentum deficit

For clarity, the typical structure of the deficit is shown again in Fig. 3 with spanwise streamlines. Inside the deficit area, there are two counter-rotating primary vortices which are illustrated in Fig. 1. In near MVG region, the shape of deficit appears to be a circle, and usually has a root connected to the boundary layer. At the underneath sides of the circle, there are two high streamwise velocity regions.
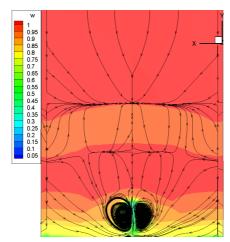
American Institute of Aeronautics and Astronautics

Figure 3. Structure of the deficit and the streamlines

Fig. 4 shows the iso-surface of pressure. Besides the expansion wave and the surface wrapping the tube near the trailing-edge, the ring-like vortex structures are found in the subsequent downstream region. Such rings appear initially not far away from the trailing-edge, and become larger and irregular when moving downstream; meanwhile the streamwise vortex tubes become weaker and disappear at a certain location.
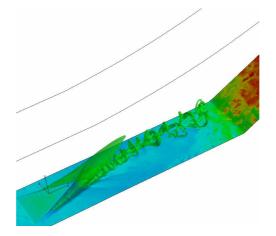

Figure 4.   The iso-surface of the instantaneous pressure

The distributions of averaged streamwise-velocity are given in Fig. 5 along the normal grid lines at the center plane. The streamwise positions of the lines are L/h ≈3.3, 6.7, 10 and 11, where L is distances from the apex of MVG. The dip of the lines corresponds to the momentum deficit, which is similar to that given by Babinsky[3].It can be seen clearly that there are at least two high shear layers in the central plane, one is located at the upper edge of the dip and the other is located at the lower edge. The second order derivative $\partial^2 w/\partial y^2$ is calculated to demonstrate the existence of the inflection points, and the result of the line at L_from_apex/h ≈ 6.7 is plotted in Fig. 6. The existence and correspondence of the inflection points at the upper and lower shear layer is illustrated by two dashed lines intersecting the distribution of the streamwise velocity and its second order derivative (Fig. 6).
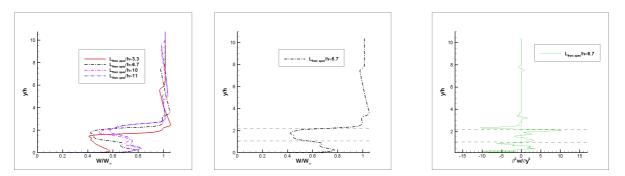
American Institute of Aeronautics and Astronautics

Figure 5. The streamwise velocity distribution at different locations

Figure 6. The distribution of the streamwise velocity (left) and its second order derivative (right) to y coordinate at L from apex/h ≈ 6.7

It is obvious that the existence of the inflection points in shear layers will cause the flow instability and generates vortex rollers according to the Kelvin-Helmholtz instability (K-H) theorem in 2D. So the mechanism for the vortex ring generation may be caused K-H type instability, and the lost of the stability of the shear layer will result in the formation of the vortex rings. Since the analysis of K-H instability is based on 2D, but our results show a complicated 3D case, so, to further explore the mechanism of the vortex ring, we developed an axisymmetric instability analysis which could be considered as a 3D instability.

II. Instability Analysis

The instability analysis is composed by two situations: incompressible flow and compressible but inviscid flow. The purpose of the arrangement of the analysis is due to that we have mainly two major dimensionless parameters, Reynolds number and Mach number, it will be easier if we discuss only one of them separately. On the other hand, although inviscid K-H type instability is considered as the dominant mechanism of the instability in our case, we still need to discuss the effect of viscosity to some extent.

A. Compressible K-H type instability

Firstly, according to the distribution of the streamwise velocity at the upper boundary of the deficit in Fig 6, we assume there is an axisymmetric flow,

$$\mathbf{U}(r) = [\frac{U_1 + U_2}{2} + \frac{U_1 - U_2}{2}\tanh(\frac{r}{\delta})]\mathbf{i} \qquad (1)$$

With two constant velocities $U_1 > U_2$ as shown in Fig. 7, and **i** defines as the unit vector in the streamwise direction.
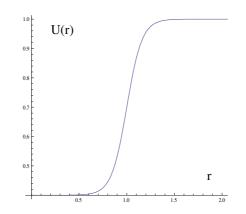
American Institute of Aeronautics and Astronautics

Figure 7. Configuration of the axisymmetric shear layer

The parameter δ here is used to adjust the curve of (1) to approach the real distribution of the streamwise velocity and it is set as 0.16 to fit our LES case.

If the disturbed flow is compressible but inviscid in both inside and outside the momentum deficit region, the governing equation can be described by inviscid Euler equations,

$$
\begin{cases}
\dfrac{\partial \rho}{\partial t} + \nabla \cdot (\rho \mathbf{u}) = 0 \\[2mm]
\rho \dfrac{D\mathbf{u}}{Dt} = -\nabla p \\[2mm]
\rho \dfrac{De}{Dt} + p(\nabla \cdot \mathbf{u}) = -\nabla \cdot \mathbf{q}
\end{cases}
\tag{2}
$$

where, ρ is the density, $\mathbf{u}$ is the velocity vector, p is the pressure, $\mathbf{q}$ denotes the heat transfer. A perfect gas obeys the perfect gas equation of state,

$$
p = \rho RT
\tag{3}
$$

We conduct the compressible but inviscid instability analysis which extends the standard 2D K-H instability analysis to the axisymmetric cases. The derivation starts from the inviscid dimensionless Euler equations in cylindrical coordinate system (which should also be axisymmetric),

$$
\begin{cases}
\dfrac{\partial \rho}{\partial t} + \dfrac{\partial \rho u_r}{\partial r} + \dfrac{\rho u_r}{r} + \dfrac{\partial \rho u_x}{\partial x} = 0 \\[2mm]
\rho[\dfrac{\partial u_r}{\partial t} + u_r \dfrac{\partial u_r}{\partial r} + u_x \dfrac{\partial u_r}{\partial x}] = -\dfrac{\partial p}{\partial r} \\[2mm]
\rho[\dfrac{\partial u_x}{\partial t} + u_r \dfrac{\partial u_x}{\partial r} + u_x \dfrac{\partial u_x}{\partial x}] = -\dfrac{\partial p}{\partial x} \\[2mm]
\rho[\dfrac{\partial T}{\partial t} + u_r \dfrac{\partial T}{\partial r} + u_x \dfrac{\partial T}{\partial x}] = [\dfrac{\partial p}{\partial t} + u_r \dfrac{\partial p}{\partial r} + u_x \dfrac{\partial p}{\partial x}](\gamma - 1)Ma^2 \\[2mm]
\gamma Ma^2 p = \dfrac{T}{T_0} + \dfrac{\rho}{\rho_0}
\end{cases}
\tag{4}
$$

where, T is the temperature, γ is the heat ratio and Ma is the mach number. The subscript 0 represents the value of free stream flow.

Consider that $q(x,r,t) = q_0(r) + q'(x,r,t)$ in which q can be specified as (u_r, u_x, T, p) and $q_0 = (U_0, T_0, P_0)$, then the governing equation for small perturbations will be,

$$\begin{cases} \rho_0[\dfrac{\partial u'_r}{\partial t} + u_x \dfrac{\partial u'_r}{\partial x}] = -\dfrac{\partial p'}{\partial r} \\[2mm] \rho_0[\dfrac{\partial u'_x}{\partial t} + u'_r \dfrac{\partial u_x}{\partial r} + u_x \dfrac{\partial u'_x}{\partial x}] = -\dfrac{\partial p'}{\partial x} \\[2mm] \rho_0[\dfrac{\partial T'}{\partial t} + u'_r \dfrac{\partial T_0}{\partial r} + u_x \dfrac{\partial T'}{\partial x}] = (\gamma-1)Ma^2[\dfrac{\partial p'}{\partial t} + u_r \dfrac{\partial p_0}{\partial r} + u_x \dfrac{\partial p'}{\partial x}] \\[2mm] T_0\gamma Ma^2 \dfrac{\partial p'}{\partial t} + u_x T_0 \gamma Ma^2 \dfrac{\partial p'}{\partial x} - \dfrac{\partial T'}{\partial t} - u_x \dfrac{\partial T'}{\partial x} - u'_r \dfrac{\partial T_0}{\partial r} + T_0 \dfrac{\partial u'_r}{\partial r} + \dfrac{T_0 u'_r}{r} + T_0 \dfrac{\partial u'_x}{\partial x} \end{cases} \tag{5}$$
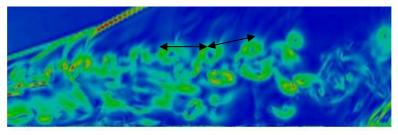

Figure 8. Scalar field of the gradient of pressure behind the MVG

For our problem, the spatial disturbance is easy to measure. Actually, it relates to the distance among two neighboring vortices in the central streamwise plane (as shown by scalar field of the gradient of pressure behind the MVG in Fig 8). So, the temporal mode is used for the stability analysis. Assume the normal mode is

$$q' = \hat{q}(r)e^{i(\beta x - \omega t)}, \tag{6}$$

where $q = (u_r, u_x, T, p)$ and the parameter β is given (which is real and set to be 6.0), ω should be a complex number. Equation (5) can be rewritten as,

$$\begin{cases} i\hat{\omega}\hat{u}_r = -T_0 D\hat{p} \\[2mm] i\rho_0\hat{u}_x + \hat{u}_r Du_{0x} = -i\beta T_0 \hat{p} \\[2mm] i\hat{\omega}\hat{T} + \hat{u}_r DT_0 = i(\gamma-1)T_0 Ma^2 \hat{\omega}\hat{p} \\[2mm] T_0 D\hat{u}_r = -i\gamma T_0 Ma^2 \hat{\omega}\hat{p} + i\hat{\omega}\hat{T} - iT_0\beta\hat{u}_x + (DT_0 - \dfrac{T_0}{r})\hat{u}_r \end{cases} \tag{7}$$

where $\hat{\omega} = \beta u_x - \omega$, and $D = \dfrac{d}{dr}$

By eliminating u_r and T we can obtain the instability equation related on pressure,

$$\hat{\omega}T_0 D^2 \hat{p} + [\hat{\omega}DT_0 - 2\beta T_0 Du_x + \dfrac{\hat{\omega}T_0}{r}]D\hat{p} + [Ma^2\hat{\omega}^3 - \hat{\omega}\beta^2 T_0]\hat{p} = 0 \tag{8}$$

The base velocity profile is given in equation (1), and the relation between temperature and velocity comes from Buesmann-Crocco's equation[6],

$$\dfrac{d^2 T_0}{dU^2} = -(\gamma-1)Ma^2 \tag{9}$$

Then the relation between temperature profile and velocity can be easily obtained according to the conditions given by Fig 7,

$$T_0 = T^* \frac{1-U}{1-U^*} + \frac{U-U^*}{1-U^*} + \frac{1}{2}(\gamma-1)Ma^2(1-U)(U-U^*) \qquad (10)$$

where, $T^* = T_1/T_2$ - the quotient of the temperature outside and inside the momentum deficit region, and $U^* = U_1/U_2$.
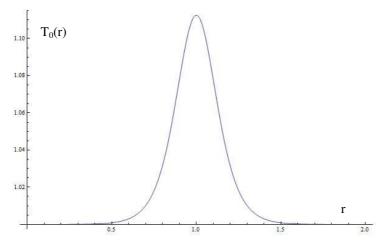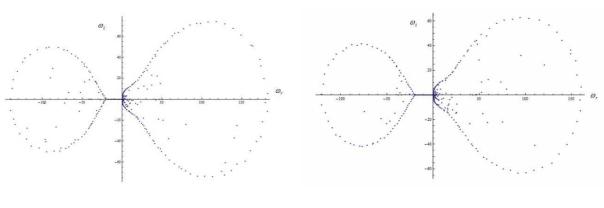

Figure 9. The Temperature profile

The second order central difference scheme is used to derive the finite different equation from equation (8),

$$(D^2\hat{p})_j = \frac{\hat{p}_{j+1} - 2\hat{p}_j + \hat{p}_{j-1}}{(\Delta r)^2}, \quad (D\hat{p})_j = \frac{\hat{p}_{j+1} - \hat{p}_{j-1}}{2\Delta r} \qquad (11)$$

Then a so called eigenvalue method is applied to get the value for ω which should be a complex number. According to the normal mode in Eq. (6), it shows that if the imaginary part of ω, ω_i, is positive, the flow is unstable, but it will be stable if ω_i is negative.

With the global method, basically, the amount of the solutions of ω from the difference equation of (8) is determined by how many numerical grids that have been used. Fig 10 shows the distribution of these solutions on the complex plane when 100 and 110 grids are used,

(a) n=100   (b) n=110

Figure 10. Distribution of solutions of ω with different grids

Although all of the solutions above are the solutions of equation (8), most of them are nonphysical. To distinguish the physical and nonphysical solutions, there are two criterions in generally. First, the nonphysical solutions will usually stick to each other. In Fig 10, many solutions form a bow, and all of

these points should not be the physical ones. Second, the physical solutions will not change their values while the quantity of grids is changed.

By the two criterions described above, we can get the physical solution of the frequency ω, as illustrated in the Fig 11 which is locally enlarged by Fig 10, whose imaginary part ω_i is about 0.44 for our case. The positive value means this kind of flow is unstable. Fig 12 shows the corresponding shape function of $\hat{p}(r)$ which is similar to those found in boundary layer flows (T-S waves),
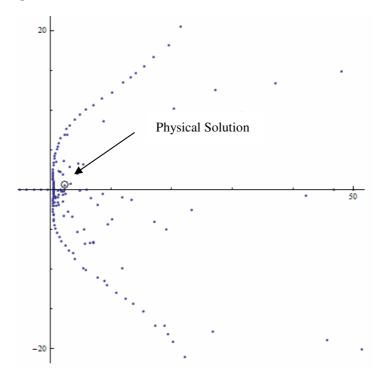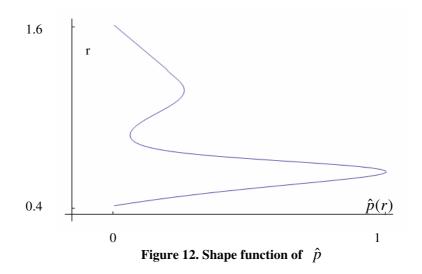
Figure 11. Distribution of solutions of ω near the origin

Figure 12. Shape function of $\hat{p}$

B. The effect of viscosity

Next, the effect of viscosity is also considered. To simplify the analysis, we assume the flow as incompressible. If the disturbed flow is incompressible in both inside and outside the momentum deficit area, then the governing equation can be described as follows.

$$\begin{cases} \dfrac{\partial \mathbf{u}}{\partial t} + (\mathbf{u} \cdot \nabla)\mathbf{u} + \nabla p = \dfrac{1}{\mathrm{Re}} \nabla^2 \mathbf{u} \\ \nabla \cdot \mathbf{u} = 0 \end{cases} \tag{12}$$

where, Re is the Reynold's number which is about 9218 if the height of the MVG is considered as the reference length scale.

For linear stability, considering the instantaneous flow q as the sum of base flow q_0 and the disturbance q', we can express

$$\begin{cases} \mathbf{u} = \mathbf{u}_0 + \mathbf{u}' \\ p = p_0 + p' \end{cases} \tag{13}$$

where $\mathbf{u}'$, p' are the small perturbations.

If all the second order terms are omitted, the equations for the small perturbations will be

$$\begin{cases} \dfrac{\partial \mathbf{u}'}{\partial t} + (\mathbf{u}_0 \cdot \nabla)\mathbf{u}' + (\mathbf{u}' \cdot \nabla)\mathbf{u}_0 + \nabla p' = \dfrac{1}{\mathrm{Re}} \nabla^2 \mathbf{u}' \\ \nabla \cdot \mathbf{u}' = 0 \end{cases} \tag{14}$$

This is a fundamental equation in the linear stability theory.

A cylindrical coordinate system (x, r, θ) is used for our problem, $u = (u_r, u_\theta, u_x)$. Since it's axisymmetric, we have $\partial / \partial \theta = 0$, $u_\theta = 0$, and the system (14) can be expressed as

$$\begin{cases} \dfrac{\partial u'_r}{\partial t} + u_x \dfrac{\partial u'_r}{\partial x} + \dfrac{\partial p'}{\partial r} = \dfrac{1}{\mathrm{Re}} [\dfrac{\partial^2 u'_r}{\partial r^2} + \dfrac{\partial^2 u'_r}{\partial x^2} + \dfrac{1}{r} \dfrac{\partial u'_r}{\partial r} - \dfrac{u'_r}{r^2}] \\ \dfrac{\partial u'_x}{\partial t} + u_x \dfrac{\partial u'_x}{\partial x} + u'_r \dfrac{\partial u'_x}{\partial r} + \dfrac{\partial p'}{\partial x} = \dfrac{1}{\mathrm{Re}} [\dfrac{\partial^2 u'_x}{\partial r^2} + \dfrac{\partial^2 u'_x}{\partial x^2} + \dfrac{1}{r} \dfrac{\partial u'_x}{\partial r}] \\ \dfrac{\partial u'_r}{\partial r} + \dfrac{u'_r}{r} + \dfrac{\partial u'_x}{\partial x} = 0 \end{cases} \tag{15}$$

in the cylindrical coordinate system.

By the method of normal modes, we assume that an arbitrary disturbance can be resolved into modes of the form,

$$\phi' = \hat{\phi}(r) e^{i(\beta x - \omega t)} \tag{16}$$

here ϕ is (u_r, u_x, p). By plugging in (16), the system (15) can be rewritten as

$$\begin{cases} L\hat{u}_r = \dfrac{1}{r^2} \hat{u}_r + \mathrm{Re} \cdot D\hat{p} \\ L\hat{u}_x = \mathrm{Re}(Du_x)\hat{u}_x + i\beta \mathrm{Re}\, \hat{p} \\ (D + \dfrac{1}{r})\hat{u}_r + i\beta \hat{u}_x = 0 \end{cases} \tag{17}$$

the operators are defined as $L = \{ D^2 - \beta^2 + \dfrac{1}{r} D - i\mathrm{Re}(\beta u_x - \omega) \}$ and $D = \dfrac{d}{dr}$

By eliminating $\hat{p}$ and $\hat{u}_r$, we can get the stability equation for our problem,

$$DL(D+\frac{1}{r})\hat{u}_r - \beta^2 L\hat{u}_r = -i\beta \operatorname{Re}[D^2 u_x \hat{u}_r + Du_{0x} D\hat{u}_r] - \frac{\beta^2}{r^2}\hat{u}_r \qquad (18)$$

Second order central difference scheme is again used to derive the finite different equation from equation (18),

$$(D^4 \hat{u}_r)_j = \frac{\hat{u}_{r\,j+2} - 4\hat{u}_{r\,j+1} + 6\hat{u}_{r\,j} - 4\hat{u}_{r\,j-1} + \hat{u}_{r\,j-2}}{(\Delta r)^4} \qquad (19)$$

$$(D^2 \hat{u}_r)_j = \frac{\hat{u}_{r\,j+1} - 2\hat{u}_{r\,j} + \hat{u}_{r\,j-1}}{(\Delta r)^2}, \quad (D\hat{u}_r)_j = \frac{\hat{u}_{r\,j+1} - \hat{u}_{r\,j-1}}{2\Delta r} \qquad (20)$$

Using the same method discussed above, the value of ω_i can be obtained, which is about 0.026 Although ω_i is much smaller, the flow is still unstable. The difference between inviscit and viscous flow instability is relatively large.

C. Numerical and Experimental Results of Vortex Rings

Since the value of ω_i is positive in both situations discussed above, the flow around the boundary of momentum deficit should be unstable due to the shear layer illustrated in Fig 6. by our LES simulation. Because invicid instability is essential to shear layer, also, the Reynold's number is greater than 9000 and mach number is 2.5, the viscosity effect is only applied to make the flow be less unstable, so the dominant mechanism for the vortex ring generation should be the K-H type instability, and the lost of the stability of the shear layer will result in the formation of the vortex rings axial symmetrically, since the shear layer around the momentum deficit area is nearly a circle.

To reveal the coherent structure of the flow, the iso-surface of λ_2 scalar field is given in Figs. 13 and 14 by LES and Experiment. It is very clear that there is a chain of vortex rings, which start from the trailing-edge of MVG. The rings are placed erectly and in a good round shape in the initial stage, then they begin to deform when propagating downstream.
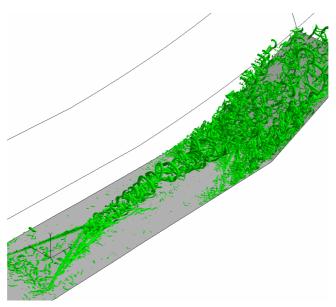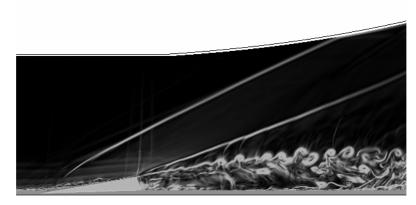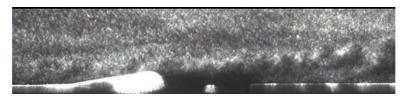

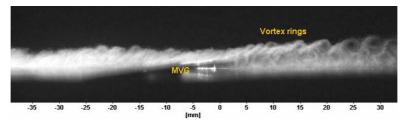**Figure 13. Vortex rings shown by iso-surface of λ₂**

a) LES

b) Using PIV

c) Using the acetone vapor

Figure 14   The laser-sheet flash image at the center plane

From further analysis, we find that the first ring is formed when the hairpin vortex travels. Consequently, multiple rings are generated at almost same time. These rings could dominant the mechanism of MVG for control of shock boundary layer interaction.

III. Conclusions

Based on our DNS and theoretical study, the following conclusions can be made.

1.   Instability analysis is made for the shear layers around the boundary of the momentum deficit generated by micro vortex generator for both incompressible viscous flow and compressible inviscid flow. The results show that the shear layers around the momentum deficit is unstable.
2.   The dominant mechanism for the vortex ring generation which has been observed by our LES and experiment should be K-H type instability, and the lost of the stability of the shear layer will result in the formation of the vortex rings axial symmetrically, which is verified by the numerical result shown by iso-surface of λ_2 and experiment.

Acknowledgements

Reference

[1]C. Liu and L. Chen, "Study of Mechanism of Ring-Like Vortex Formation in Late Flow Transition," *AIAA Paper 2010-1456.*

[2]Q. Li and C. Liu, "Numerical Investigations on the Effects of the Declining angle of the trailing-edge of MVG," *AIAA paper 2010-714.*

[3]H. Babinsky, Y. Li, and C. W. Pitt Ford, "Microramp Control of Supersonic Oblique Shock-Wave/Boundary-Layer Interactions," *AIAA J.*, Vol. 47, No. 3, 2009, pp.668-675.

[4]S. Ghosh, J. Choi and J. R. Edwards, "RANS and Hybrid LES/RANS Simulations of the Effects of Micro Vortex Generators Using Immersed Boundary Methods," *AIAA paper 2008-3726.*

[5]S. Lee, E. Loth and C. Wang, "LES of Supersonic Turbulent Boundary Layers with μVG's," *AIAA Paper 2007-3916.*

[6]Sandham ND and Renolds WC, "Compressible mixing layer: linear theory and direct simulation," *AIAA J*, Vol. 28, 1990, pp.618-624.

[7]G. Jiang and C. W. Shu, "Efficient Implementation of Weighted ENO Schemes," *J. Comput. Phys.*, Vol. 126, 1996, pp.202–228.

[8]Charles W. Pitt Ford and Holger Babinsky, "Micro-Ramp Control for Oblique Shock Wave/Boundary Layer Interaction," *AIAA paper 2007-4115.*

[9]H. Holden and H. Babinsky, "Effect of Microvortex Generators on Separated Normal Shock/Boundary Layer Interactions," *AIAA J.*, 2007, pp.170-173.

[10]S. Lee and E. Loth, "Supersonic Boundary Layer Interactions with Various Micro-Vortex Generator Geometries," *AIAA Paper 2009-3712.*

[11]D. S. Dolling and M. T Murthy, "Unsteadiness of the Separation Shock Wave Structure in a Supersonic Compression Ramp Flowfield," *AIAA J.*, Vol. 12, 1983, pp.1628-1634.

[12]D. S. Dolling, "High-Speed Turbulent Separated Flows: Consistency of Mathematic Models and Flow Physics," *AIAA J.*, Vol. 36, 1998, pp. 725-732.